materials

MDPI

Article

Effect of Ion Corrosion on 517 Phase Stability

Guijia Wang [1], Zhiqi Hu [1], Jun Chang [2], Yan Guan [1], Tingting Zhang [2] and Wanli Bi [1,3,*]

[1] Institute of Materials and Metallurgy, University of Science and Technology Liaoning, Anshan 114031, China; anshanwgj@126.com (G.W.); Anshanhzq@126.com (Z.H.); guanyan@ustl.edu.cn (Y.G.)
[2] Faculty of Infrastructure Engineering, Dalian University of Technology, Dalian 116024, China; mlchang@dlut.edu.cn (J.C.); tingtingzhang@dlut.edu.cn (T.Z.)
[3] Research Institute of Keda Fengchi Magnesium Building Materials, Anshan 114031, China
* Correspondence: biwanli@ustl.edu.cn

Received: 13 November 2020; Accepted: 9 December 2020; Published: 11 December 2020

Abstract: The main hydration product and source of strength of magnesium oxysulfate cement is $5Mg(OH)_2 \cdot MgSO_4 \cdot 7H_2O$ (known as the 517 phase). Hardened pastes containing 92.38% of the 517 phase were synthesized in this study, and the influence of different types of chloride solutions on the stability and compressive strength of the 517 phase was investigated. X-ray diffraction and the Rietveld method were used to investigate the 517 phase transition in chloride solutions. Ion chromatography and inductively coupled plasma spectrometry were used to analyze the ion concentrations of the chloride solutions. Scanning electron microscopy and mercury injection porosimetry were used to investigate the effect of ion erosion on the microstructure and pore size distribution. The results showed that the crystal structure of 517 phase remained stable upon immersion in chloride solutions (except for the $CaCl_2$ solution) up to 28 days, and there was no discernible attenuation in the compressive strength of the hardened pastes. Immersion of the 517 phase in $CaCl_2$ solution for 28 days caused Ca^{2+} ions to combine with SO_4^{2-} groups to generate $CaSO_4 \cdot 2H_2O$, thereby decomposing the 517 phase. An increase in the concentration of magnesium and sulfate ions in the immersion solutions confirmed the decomposition of the 517 phase. Gel-like $Mg(OH)_2$ was observed in the microstructure of the decomposed 517 phase, and the decomposition of the 517 phase increased the porosity of the hardened pastes.

Keywords: 517 phase; magnesium oxysulfate cement; ion corrosion; mechanical properties; microstructure

1. Introduction

Magnesium oxysulfate (MOS) cement is a gas-hardened magnesium cementitious material prepared from active magnesium oxide and a magnesium sulfate aqueous solution [1,2]. MOS cement has the advantages of a light weight, a short setting time [3], and low alkalinity, while providing thermal insulation [4], energy saving, and environmental protection with a low corrosion rate for steel [5]. MOS cement is widely used in light fireproofing and building materials [6]. Unlike magnesium oxychloride (MOC) cement, MOS cement does not does not contain chloride ions and, therefore, does not significantly corrode steel bar; the corrosion rate of MOS cement is even lower than that of Portland cement in the late stages of hydration, such that MOS cement can be used to prepare reinforced concrete. However, poor water resistance limits offshore engineering applications of MOS cement [1,2,6–8].

In recent studies, the effect of 517 phase formation on the mechanical properties of MOS cement has been widely investigated. Studies have shown that the 517 phase is an important hydration product of MOS cement. The main method of forming the 517 phase, which increases the strength of MOS cement, is to add a weak acid or a weak acid salt to MOS cement. For example, adding citric

acid, sodium citrate [9], tartaric acid [10], and phosphoric acid [6] to MOS cement can significantly improve the mechanical strength and water resistance by promoting the formation of the 517 phase. Additionally, some studies also focused on the stability of 517 phase. Runcevski et al. [2] studied the thermal stability and decomposition of the 517 phase. The 517 phase was found to be stable from 52 °C to 90 °C, and decomposed at or above 90 °C. Ba et al. [11] found that the 517 phase remained stable after carbonation of MOS cement. Zhao [12] showed that the 517 phase was stable in an alkaline solution with pH ≤11 and began to decompose at pH >12, deteriorating the mechanical properties of MOS cement. Wang et al. [13] tested the phase composition and mechanical properties of a hardened paste of MOS cement under dry–wet cycle conditions and found that the 517 phase was stable.

In summary, numerous studies have been conducted on improving the performance of MOS cement and the stability of the hydration product (the 517 phase) both in China and abroad; however, comparatively few studies have been carried out to investigate how ion erosion affects the stability of the 517 phase. The stability of the 517 phase subjected to erosion ions was investigated in this study to expand the application range of MOS cement, especially in the field of marine engineering. A hardened paste of the pure 517 phase was synthesized and characterized, and the compressive strength of the hardened paste was compared after soaking the hardened paste in different chloride solutions. The transformation of the 517 phase during erosion was investigated using X-ray diffraction (XRD) and the Rietveld method, and ion chromatography (IC) and inductively coupled plasma spectrometry (ICP) were used to determine the ion concentration in the solution before and after soaking. The microstructure and pore diameter distribution of the 517 phase before and after soaking in chloride solutions were determined using SEM and mercury intrusion porosimetry (MIP).

2. Experiment

2.1. Preparation of Raw Materials and Hardened Paste

Figure 1 for schematic of the preparation of raw materials and hardened paste. The 517 phase was synthesized using the following procedure: 100 g of light magnesium oxide (Sinopharm Chemical Reagent Co., Ltd., Shanghai, China) and 122.3 g of magnesium sulfate heptahydrate (Yingkou Magnesite Chemical Ind Group Co., Ltd., Yingkou, China) were mixed evenly; 0.3 g of citric acid (Gongyi Meiyuan Water Purification Co., Ltd., Gongyi, China) was added to 98.3 mL of distilled water to form a solution; the mixed powder was then added to the solution and mixed for approximately 1 min; the resulting slurry was poured into a mold with dimensions of 20 mm × 20 mm × 20 mm, maintained at a temperature of 20 ± 1 °C and a humidity of 60% ± 5%, and demolded after hardening. The hardened paste of the 517 phase was then immersed in different chloride (NaCl, $CaCl_2$, $AlCl_3$, $FeCl_2$, and $FeCl_3$) solutions, controlling the concentration of chloride ions in each solution to be 3%.

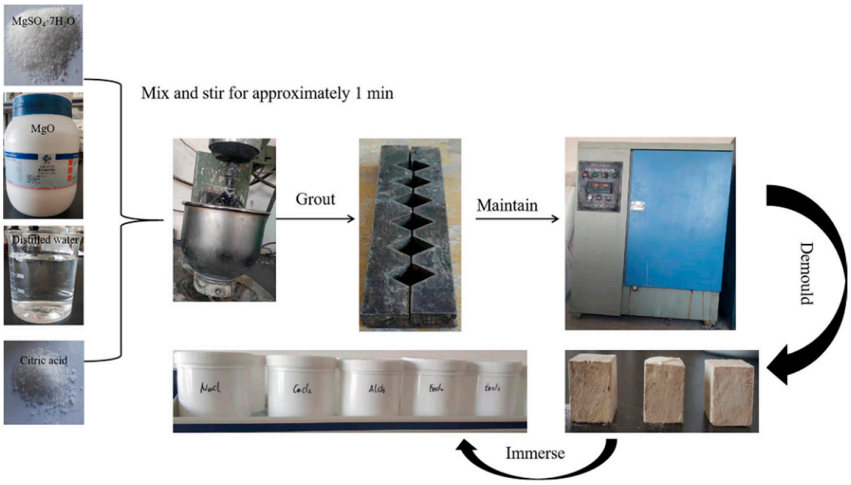

Figure 1. Schematic of the preparation of raw materials and hardened paste.

2.2. Test Methods

2.2.1. Compressive Strength

According to national standard GB175-1999, the compressive strength of hardened pastes of the synthesized 517 phase was measured using a YES-2000 universal testing machine. The loading rate was 600 N/s, and the compressive strength was determined for hardened pastes of the 517 phase that were air cured for 168 h and soaked in chloride solutions for 28 days. After a curing period of 168 h, the hardened paste of the 517 phase was immersed in different chloride solutions for a prescribed period, and the compressive strength of the sample was determined; the softening coefficient (R_f) was used to evaluate the corrosion resistance of the hardened paste of the 517 phase. Equation (1) shows the formula used to calculate R_f; to ensure accuracy, three samples were tested in parallel for each group of data, and the test results were averaged.

$$R_f = \frac{R_w}{R_a} \quad (1)$$

where R_a and R_w denote the compressive strength of the hardened paste after 168 h of curing and after soaking in a chloride solution for a prescribed time, respectively.

2.2.2. Phase Composition

The XRD and Fourier-transform infrared (FTIR) analysis methods were previously described [9,10]. The samples were analyzed using a Panaco X'pert Powder X-ray diffractometer (XRD, Panalytical X'pert power, Malvern, UK): λ_{Cu} = 0.15418 nm, tube pressure = 40 kV, tube flow = 40 mA, start angle = 5°, end angle = 85°, step size = 0.02°, and time per step = 5 s. The XRD pattern was introduced into High Score software (3.0.5 version, PANalytical B.V, Amelo, Netherlands) and compared with standard diffraction peaks to determine the composition of the 517 phase before and after immersion in the chloride solutions. The samples were then analyzed using an Agilent Technologies Cary 630 FTIR spectrometer (Agilent Technologies, Santa Clara, CA, USA), where the detected wave numbers ranged from 400 to 4000 cm^{-1}. The XRD and FTIR analyses were carried out at room temperature.

The amorphous content of the samples was quantified using an internal standard method over 2θ range of 5–85°; a zinc oxide (ZnO) analytic reagent was mixed into the test samples at 15% by mass before analysis [14]. The Rietveld method, as implemented in the Topas 6.0 software (6.0 version, Bruker, Hamburg, Germany), was used for the quantitative analysis of the mineral phases in the 517 phase samples by fitting the peak areas [14]. The Rietveld method has become a powerful tool for quantitative phase analysis by XRD maps. Taylor first used the Rietveld method in 1991 to quantitatively analyze clay minerals [15]. The amorphous contents of the samples in this study were calculated using Equation (2), where W_{st} represents the weight fraction of added ZnO, and R_{st} is the Rietveld refined weight fraction of ZnO.

$$ACn = \frac{1 - W_{st}/R_{st}}{100 - W_{st}} \times 10^4\% \quad (2)$$

The ionic compositions of the chloride solutions in which the hardened paste was immersed were measured; a Dionex ICS-3000 ion chromatograph (DIONEX, Diane, Sunnyvale, CA, USA) was used to perform a sulfate ion analysis, and a Shimadzu ICPE 9000 spectrometer (Shimadzu, Kyoto, Japonia) was used to perform a magnesium ion analysis, according to the protocol in [12].

2.2.3. Microscopic Morphology and Pore Structure

After being immersed in different solutions, the hardened paste samples of the 517 phase were cut into small pieces with sizes of 3–5 mm and soaked in alcohol to terminate hydration, followed by drying in an oven at 52 °C. The pore diameter distribution of some samples was tested using a mercury

intrusion porosimeter (MIP) Auto Pore IV 9500 (MIP, Quantachrome Autoscan 60, Boynton Beach, FL, USA). The remaining samples were analyzed using a (JSM-5610lv) scanning electron microscope (SEM, ZEISS SIGMA HD, Jena, Germany). The sample preparation, curing temperature, and test method were previously described [2].

3. Results

3.1. Characterization of Synthesized 517 Phase

Figure 2 presents the XRD test results for the synthesized hardened paste, which are similar to the Runcevski et al. [2] crystal data for the 517 phase. A quantitative Rietveld analysis was carried out using Topas 6.0 software (Figure 3). The sample contained 92.38% of the 517 phase and 7.62% of the amorphous phase. The R_{wp} was 8.3%; the good Rietveld fine fitting results indicated a 517 phase with relatively high purity. The microstructure of the hardened paste was observed. The matrix was composed of interlaced needle-like/rod-shaped crystals. The whiskers had a diameter of approximately 200–300 nm and a length of 3–5 μm, corresponding to a length-to-diameter ratio of approximately 10 to 25; the O:Mg:S atomic ratio of 72.01:23.91:4.02 was experimentally obtained by testing 30 different clusters of the synthesized 517 phase. Thus, the crystal was confirmed to be the 517 phase.

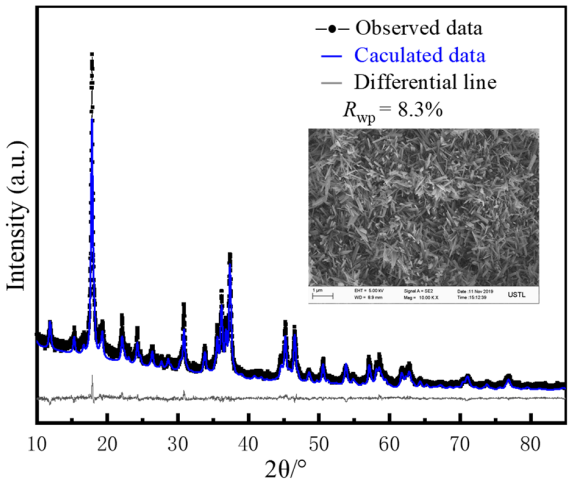

Figure 2. Synthesized hardened slurry: Rietveld diagram obtained by X-ray diffraction (XRD) and microstructure observed by SEM.

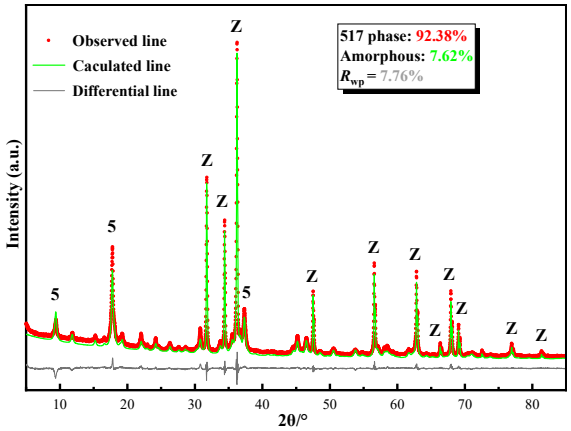

Figure 3. Quantitative Rietveld plots for synthesized hardened paste tested by external standard method: Z:ZnO, 5:517 phase.

3.2. Compressive Strength of Hardened Paste of 517 Phase

Figure 4 shows the compressive strength and softening coefficient of the hardened paste of the 517 phase after curing in air and soaking in different chloride solutions. The compressive strength of the paste after air curing was measured as 22.76 MPa. After the paste was soaked in NaCl, $AlCl_3$, $FeCl_2$, and $FeCl_3$ solutions for 28 days, the compressive strength did not decrease significantly and was 22.18 MPa, 21.38 MPa, 22.04 MPa, and 21.36 MPa, respectively, whereas the softening coefficient was 0.965, 0.926, 0.941, and 0.934, respectively. Soaking the paste in a $CaCl_2$ solution for 28 days caused the compressive strength to decrease to 12.43 MPa, and the softening coefficient was 0.548. The results presented above show that the chloride solutions, except for the $CaCl_2$ solution, had little effect on the compressive strength of the hardened paste.

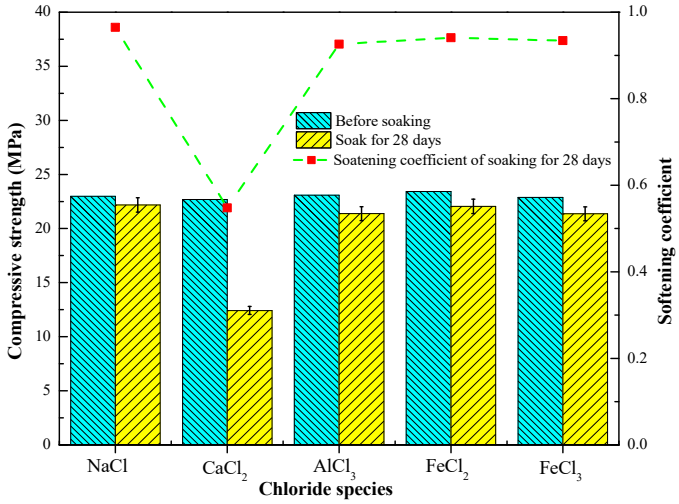

Figure 4. Compressive strength and softening coefficient of hardened pastes of 517 phase immersed in different chloride solutions for 28 days.

3.3. Transformation of 517 Phase in Chloride Solutions

Figure 5 shows the XRD pattern for the 517 phase after the hardened pastes were soaked for 28 days in different chloride solutions. The composition of the pastes before and after soaking in the chloride solutions, except for the $CaCl_2$ solution, corresponded to the 517 phase. $CaSO_4{\cdot}2H_2O$, $Mg(OH)_2$ and 517 phases were detected in the samples that were immersed in the $CaCl_2$ solution for 28 days.

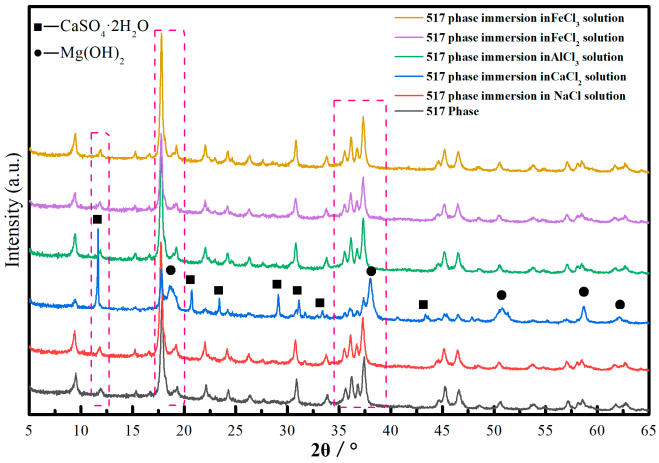

Figure 5. XRD patterns of 517 phase after immersing hardened paste in different chloride solutions for 28 days.

The phase composition was further confirmed by using the Rietveld method to analyze the XRD patterns obtained using the internal method. Figure 6 shows the fitting result for the hardened pastes of the 517 phase immersed in the $CaCl_2$ solution for 28 days. Table 1 is a comparison of the phase composition of the different samples. The chloride solutions, except for the $CaCl_2$ solution, had little effect on the 517 phase, where the 517 phase content remained above 90% after soaking for 28 days in the chloride solutions.

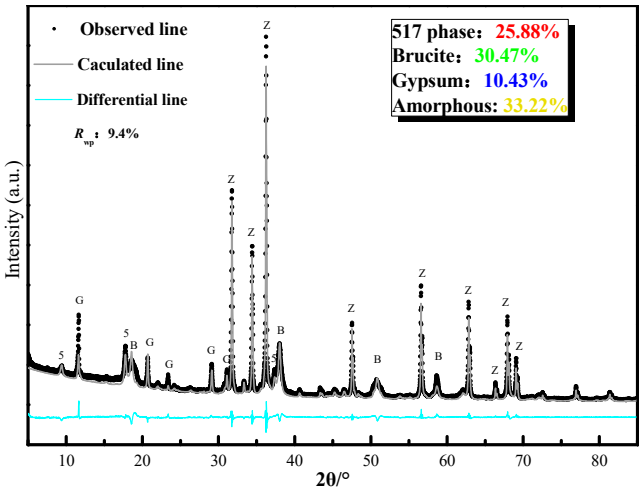

Figure 6. Rietveld fitting results for 517 phase after immersing hardened paste in $CaCl_2$ solution for 28 days; Z:ZnO, 5:517 phase, G:$CaSO_4{\cdot}2H_2O$, B:$Mg(OH)_2$.

Table 1. Contents of hardened paste of 517 phase after immersion in different chloride solutions for 28 days.

Chloride Species	Phase Composition (wt.%)			
	517 Phase	$Mg(OH)_2$	$CaSO_4{\cdot}2H_2O$	Amorphous Content
Before Soaking	92.84	0	/	7.16
NaCl	92.03	0	/	7.97
$CaCl_2$	25.88	30.47	10.43	33.22
$AlCl_3$	91.48	0	/	8.52
$FeCl_2$	91.65	0	/	8.35
$FeCl_3$	91.78	0	/	8.22

Figure 7 shows the infrared spectrum for the hardened paste of the 517 phase before and after immersion in the $CaCl_2$ solution. The 4700–2500 cm^{-1} band corresponds to crystalline water and hydroxide anion vibrational bands. The 3720 and 3640 cm^{-1} peaks are MgO–H asymmetric vibration peaks, and the 3400 cm^{-1} peak is the characteristic crystalline water stretching vibration. The 2500–470 cm^{-1} band corresponds to an HO–H vibration peak, while four other sulfate anion vibration peaks can be identified at 1100 cm^{-1}, 979 cm^{-1}, 657 cm^{-1}, and 426 cm^{-1}. After soaking the paste in $CaCl_2$ solution, the peak strength of the vibrational bands for MgO–H and crystalline water increased significantly, indicating an increase in the content of hydroxide and crystalline water in the system, which is consistent with the XRD results.

Table 2 lists the concentrations of Mg^{2+} and $SO_4{}^{2-}$ in the chloride solutions after immersion of the hardened pastes for 28 days. The Mg^{2+} and $SO_4{}^{2-}$ concentrations in the NaCl, $AlCl_3$, $FeCl_2$, and $FeCl_3$ immersion solutions were 3.97 and 0.63 mmol/L, 4.03 and 0.67 mmol/L, 3.87 and 0.66 mmol/L, and 3.93 and 0.64 mmol/L, respectively. The molar ratio of Mg^{2+} to $SO_4{}^{2-}$ was approximately 6. After immersing the hardened paste of the 517 phase in the $CaCl_2$ solution for 28 days, the Mg^{2+} and $SO_4{}^{2-}$ concentrations were 37.43 mmol/L and 32.48 mmol/L, respectively. The molar ratio of Mg^{2+} to $SO_4{}^{2-}$ was approximately 1. The 517 phase only has a solubility of 0.34 g/L in solution; therefore, only a

small quantity of Mg^{2+} and $SO_4{}^{2-}$ are dissolved in the $CaCl_2$ solution, as expressed by Equation (3). The 517 phase decomposition products are $Mg(OH)_2$, $MgSO_4$, and H_2O; as one of the decomposition products of 517 phase, magnesium sulfate is easily soluble in water, the dissolution can be described by Equation (4), where the molar ratio of Mg^{2+} to $SO_4{}^{2-}$ is equal to 1. When immersed in $CaCl_2$ solution, the Ca^{2+} ions in solution react with dissolved $SO_4{}^{2-}$ to form $CaSO_4{\cdot}2H_2O$, thereby reducing the $SO_4{}^{2-}$ concentration and accelerating the decomposition of the 517 phase, as given by Equation (5).

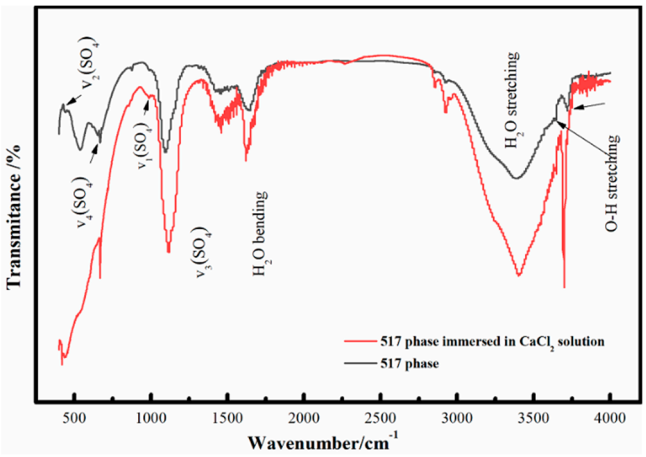

Figure 7. Infrared spectra of 517 phase before and after immersion of hardened paste in $CaCl_2$ solution.

$$5Mg(OH)_2 \cdot MgSO_4 \cdot 7H_2O \rightarrow 6Mg^{2+} + SO_4{}^{2-} + 10OH^- + 7H_2O \quad (3)$$

$$MgSO_4 \rightarrow Mg^{2+} + SO_4{}^{2-} \quad (4)$$

$$Ca^{2+} + SO_4{}^{2-} + 2H_2O = CaSO_4 \cdot 2H_2O \quad (5)$$

Table 2. Concentrations of Mg^{2+} and $SO_4{}^{2-}$ in different chloride solutions used to immerse hardened paste for 28 days.

Chloride Species	NaCl	$CaCl_2$	$AlCl_3$	$FeCl_2$	$FeCl_3$
Mg^{2+} (mmol/L)	3.97	37.43	4.03	3.87	3.93
$SO_4{}^{2-}$ (mmol/L)	0.63	32.48	0.67	0.66	0.64

3.4. Effect of Chloride Solutions on Microstructure and Pore Size Distribution of 517 Phase

Figure 8a shows a SEM image of the 517 phase before immersion in the chloride solutions. The 517 phase crystals were needle-like/rod-shaped and closely arranged in the matrix. Figure 8b shows an SEM image of the 517 phase after immersion in a NaCl solution for 28 days; there was no discernible change in the microstructure of the 517 phase, whereby the crystals remain needle-like/rod-shaped, and no other crystal formation could be observed. SEM images of the 517 phase after immersion in a $CaCl_2$ solution for 28 days are shown in Figure 8c,d; the matrix consisted of the 517 phase, $CaSO_4{\cdot}2H_2O$, and layered $Mg(OH)_2$. The morphology of the 517 phase changed, and the surface of the needle-like/rod-shaped crystals was coated with a gelatinous substance, which may be gel-like $Mg(OH)_2$, corresponding to the increase in the amorphous content of the sample, as presented in Table 1. The formation of $CaSO_4{\cdot}2H_2O$ and $Mg(OH)_2$ created an expansion stress in the matrix, resulting in expansion cracking of the sample, which was the main reason for the decrease in the compressive strength and the softening coefficient of the hardened slurry of the 517 phase [6,16,17].

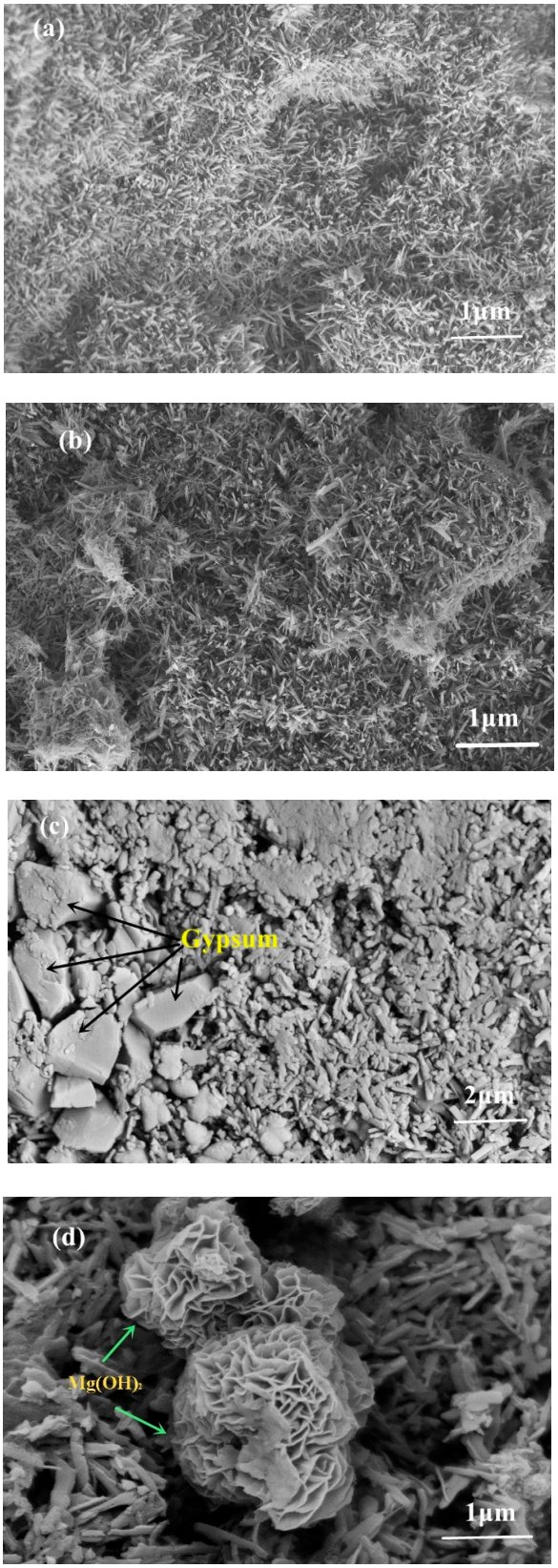

Figure 8. SEM images of 517 phase before and after soaking in different solutions: (**a**) before soaking; (**b**) after soaking in NaCl solution for 28 days; (**c**,**d**) after soaking in $CaCl_2$ solution for 28 days.

Figure 9 shows the cumulative porosity of the 517 phase before and after immersion of the hardened paste in the $CaCl_2$ solution for 28 days. The pore size of the sample after immersion was larger than before immersion, which was related to the formation of $CaSO_4 \cdot 2H_2O$ and $Mg(OH)_2$, resulting in volume expansion cracking. Figure 10 shows the pore size distribution curve before and after immersing the hardened paste of the 517 phase in the $CaCl_2$ solution. The pore size distribution before immersion consisted mainly of small capillary pores (10–100 nm), indicating that the 517 phase has good crystallinity. After immersion in the $CaCl_2$ solution, the sample contained noticeably large pores (>100 nm), and the average pore size was also larger than before immersion. It can be seen that, when the 517 phase was immersed in $CaCl_2$ solution, the number of pores between 10 nm and 100 nm was larger than before immersion, and the increase was attributed to the generation of poorly crystalline products. This corresponded to the result of the increase in the content of amorphous substance, as presented in Table 1. In addition, the increase in the volume fractions of large pores (>100 nm) had a negative effect on the compressive strength of 517 phase hardened paste. The results for the cumulative porosity and the pore size distribution show that immersing the hardened paste in the $CaCl_2$ solution increased the content of large pores and decreased the content of small capillary pores, resulting in an increase in the porosity.

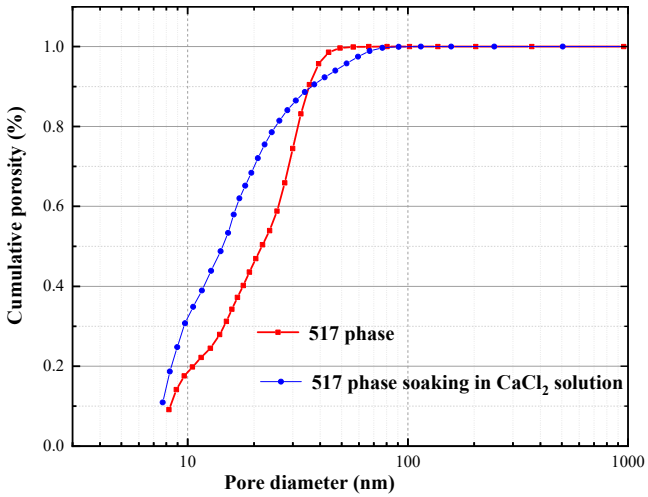

Figure 9. Cumulative porosity of hardened paste of 517 phase before and after immersion in $CaCl_2$ solution.

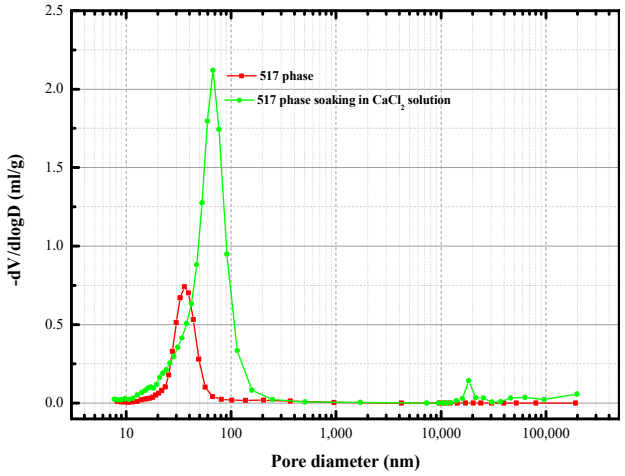

Figure 10. Pore size distribution of 517 phase before and after immersion in $CaCl_2$ solution.

4. Discussion

Many studies have shown that the 517 phase content determines the performance of magnesium sulfate cement because the 517 phase is the main contributor to the cement strength [6,7,10–12]. The test results presented above showed that the 517 phase is stable in NaCl, $AlCl_3$, $FeCl_2$, and $FeCl_3$ solutions but undergoes a decomposition reaction (Equation (6)) in a $CaCl_2$ soaking solution. The structural analysis showed that the decomposition products of the 517 phase are $Mg(OH)_2$ and $MgSO_4$, which increases the Mg^{2+} and $SO_4{}^{2-}$ concentrations in the soaking solution. Table 3 shows the $\Delta_f G_m^{\Theta}$ for each substance in the system its standard state; the values of $\Delta_f G_m^{\Theta}$ according to Equations (4) and (5) were calculated as −25.26 KJ/mol and −10.07 KJ/mol, showing that the reaction can proceed spontaneously. According to the second law of thermodynamics, chemical reactions always proceed in the direction of negative $\Delta_f G_m^{\Theta}$, and a more negative value of $\Delta_f G_m^{\Theta}$ denotes a higher likelihood of the chemical reaction to proceed [18]; thus, the probability of the chemical reactions occurring can be theoretically ranked from the magnitude and sign of the Gibbs free energy of each chemical reaction [19]. Accordingly, Ca^{2+} preferentially combines with the $SO_4{}^{2-}$ dissolved in the 517 phase in solution to form $CaSO_4{\cdot}2H_2O$, which consumes $SO_4{}^{2-}$ and accelerates the decomposition of the 517 phase. The formation of gypsum causes expansion, which leads to the appearance of large pores and cracks inside the sample and loosens the matrix, thus reducing the compressive strength. The crystal packing of the 517 phase has a characteristic laminar structure (see Figure 11), and the main blocks consist of infinite triple chains of MgO_6 octahedra. Between the laminar structures, the stability of the structure is maintained by some charge equilibrium, and the reaction between the Ca^{2+} and the sulfate destroys the equilibrium, which leads to the decomposition of the 517 phase. Other crystals, characterized by a laminar structure, exhibit a similar tendency, such as mono-sulfur sulfoaluminate, which shows a change in its crystal structure in specific environments [20].

$$5Mg(OH)_2 \cdot MgSO_4 \cdot 7H_2O \rightarrow Mg^{2+} + SO_4{}^{2-} + 5Mg(OH)_2 + 7H_2O \quad (6)$$

Table 3. Standard molar thermodynamic properties of solid phases at 298.15 K.

Solids	$\Delta_f G_m^{\Theta}/(\mathrm{KJ{\cdot}mol^{-1}})$	$\Delta_f H_m^{\Theta}/(\mathrm{KJ{\cdot}mol^{-1}})$	$S_m^{\Theta}/(\mathrm{J{\cdot}mol^{-1}{\cdot}K^{-1}})$	Ref.
$Mg(OH)_2$	−831.31 ± 0.11	−921.62 ± 0.11	63.18	[21]
517 Phase	−7026.43 ± 7.40	−7998.61 ± 3.60	674.32 ± 13.00	[21]
$CaSO_4{\cdot}2H_2O$	−1797.62	−2032.44	162.55	[22]
Ca^{2+} (aq)	−553.60	−542.80	−53.10	[22]
H_2O (l)	−237.13	−285.83	69.91	[22]
Mg^{2+}	−454.80	−466.90	−138.10	[22]
$SO_4{}^{2-}$ (aq)	−744.50	−909.30	210.10	[22]

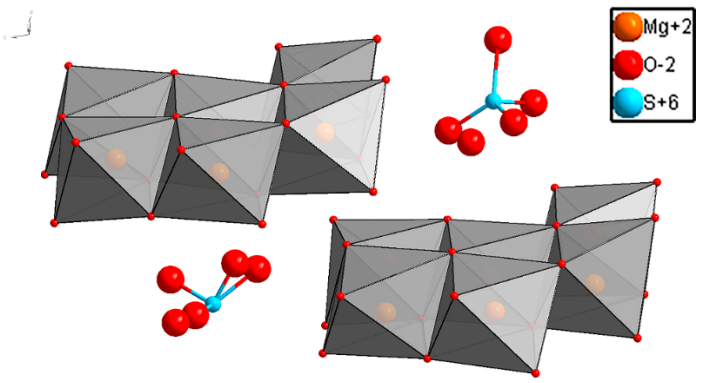

Figure 11. Crystal structure of 517 phase.

5. Conclusions

In this study, the effect of different chloride solutions on the compressive strength, phase transition, and microstructure of the 517 phase was investigated, and the following conclusions were obtained:

1. The compressive strength of the 517 phase remained stable in NaCl, $AlCl_3$, $FeCl_2$, and $FeCl_3$ solutions but decreased to 12.43 MPa after soaking in a $CaCl_2$ solution for 28 days.
2. Immersing the hardened paste in the $CaCl_2$ solution caused the 517 phase to decompose into $Mg(OH)_2$, $MgSO_4$, and H_2O. According to the second law of thermodynamics, Ca^{2+} preferentially reacted with SO_4^{2-} to form gypsum, which broke the charge balance of the 517 phase and destroyed its laminar structure, thereby leading to 517 phase decomposition, as reflected by the decrease in 517 phase content in harden pastes and the obvious increase in concentrations of Mg^{2+} and SO_4^{2-} in immersing solutions. When immersed in other chloride solutions, the 517 phase was stable and no new substance was formed.
3. The formation of gypsum increased the content of large pores (>100 nm), while the decomposition of the 517 phase was accompanied by the appearance of some amorphous materials with poor crystallization, which enlarged the pore size (10–100 nm), thereby increasing the porosity of the hardened paste.

Author Contributions: Conceptualization, G.W., Z.H., J.C., Y.G., T.Z., and W.B.; methodology, G.W., Z.H., J.C., Y.G., T.Z., and W.B.; formal analysis, G.W., Z.H., J.C., Y.G., T.Z., and W.B.; investigation, G.W., Z.H., J.C., T.Z., and W.B.; resources, Y.G. and W.B.; writing—original draft preparation, G.W., Z.H., J.C., T.Z., and W.B.; writing—review and editing, G.W., Z.H., J.C., T.Z., and W.B.; supervision, G.W., Z.H., J.C., Y.G., T.Z., and W.B. All authors have read and agreed to the published version of the manuscript.

Funding: This research was funded by the National Natural Science Foundation of China with Grant No. 51778101 and the Natural Science Foundation of Liaoning province with Grant No.2020-MS-115.

Conflicts of Interest: The authors declare no conflict of interest.

References

1. Walling, S.A.; Provis, J.L. Magnesium-based cements: A journey of 150 years, and cements for the future. *Chem. Rev.* **2016**, *116*, 4170–4204. [CrossRef]
2. Runčevski, T.; Wu, C.Y.; Yu, H.F.; Yang, B.; Dinnebier, R. Structural characterization of a new magnesium oxysulfate hydrate cement phase and its surface reactions with at pheric carbon dioxide. *J. Am. Ceram. Soc.* **2013**, *96*, 3609–3616. [CrossRef]
3. Zhou, X.; Li, Z. Light-weight wood–magnesium oxychloride cement composite building products made by extrusion. *Constr. Build. Mater.* **2012**, *27*, 382–389. [CrossRef]
4. Dang, L.; Nai, X.Y.; Dong, Y.P.; Li, W. Functional group effect on flame retardancy, thermal and mechanical properties of organophosphorus-based magnesium oxysuflate whisker as a flame retardant in polypropylene. *Rsc Adv.* **2017**, *7*, 21655–21665. [CrossRef]
5. Kahle, K. Mechanism formation of magnesium-sulfate cements. *Silikatechnik* **1972**, *23*, 148–151.
6. Wu, C.; Yu, H.; Zhang, H.; Dong, J.; Wen, J.; Tan, Y. Effects of phosphoric acid and phosphates on magnesium oxysulfate cement. *Mater. Struct.* **2013**, *48*, 907–917. [CrossRef]
7. Wu, C.Y. Fundamental Theory and Civil Engineering Application of Basic Magnesium Sulfate Cement. Ph.D. Thesis, The University of Chinese Academy of Sciences, Beijing, China, April 2014.
8. Wu, C.; Yu, H.; Dong, J.; Zheng, L. Effects of Material Ratio, Fly Ash, and Citric Acid on Magnesium Oxysulfate Cement. *ACI Mater. J.* **2014**, *111*, 291–297. [CrossRef]
9. Wang, N.; Yu, H.; Bi, W.; Tan, Y.; Zhang, N.; Wu, C.; Ma, H.; Hua, S. Effects of sodium citrate and citric acid on the properties of magnesium oxysulfate cement. *Constr. Build. Mater.* **2018**, *169*, 697–704. [CrossRef]
10. Wu, C.; Chen, W.; Zhang, H.; Yu, H.; Zhang, W.; Jiang, N.; Liu, L. The hydration mechanism and performance of Modified magnesium oxysulfate cement by tartaric acid. *Constr. Build. Mater.* **2017**, *144*, 516–524. [CrossRef]
11. Ba, M.; Xue, T.; He, Z.; Wang, H.; Liu, J. Carbonation of magnesium oxysulfate cement and its influence on mechanical performance. *Constr. Build. Mater.* **2019**, *223*, 1030–1037. [CrossRef]

12. Zhao, J.Y.; Xu, J.H.; Cui, C.Y. Stability and phase transition of 517 phase in alkaline solutions. *Constr. Build. Mater.* **2020**, *258*, 119683. [CrossRef]
13. Wang, R.; Qin, L.; Gao, X. Mechanical strength and water resistance of magnesium oxysulfate cement based lightweight materials. *Cem. Concr. Compos.* **2020**, *109*, 103554. [CrossRef]
14. Gualtieri, A.F. Accuracy of XRPD QPA using the combined Rietveld–RIR method. *J. Appl. Crystallogr.* **2000**, *33*, 267–278. [CrossRef]
15. Taylor, J.C. Computer programs for standard less quantitative analysis of minerals using the full powder diffraction profile. *Powder Diffr.* **1991**, *6*, 2–9. [CrossRef]
16. He, P.; Poon, C.S.; Tsang, D.C. Comparison of glass powder and pulverized fuel ash for improving the water resistance of magnesium oxychloride cement. *Cem. Concr. Compos.* **2018**, *86*, 98–109. [CrossRef]
17. Mo, L.; Deng, M.; Tang, M.; Al-Tabbaa, A. MgO expansive cement and concrete in China: Past, present and future. *Cem. Concr. Res.* **2014**, *57*, 1–12. [CrossRef]
18. Li, X.; Tan, P.; Lu, W.; Liu, G.; Peng, Z.; Zhou, Q. Sintering process between kaolinite and alkali lime. *JCCS* **2006**, *34*, 422–426.
19. Luong, V.-T.; Kang, D.J.; An, J.W.; Kim, M.J.; Tran, T. Factors affecting the extraction of lithium from lepidolite. *Hydrometallurgy* **2013**, *134*, 54–61. [CrossRef]
20. Baquerizo, L.G.; Matschei, T.; Scrivener, K.; Saeidpour, M.; Wadsö, L. Hydration states of AFm cement phases. *Cem. Concr. Res.* **2015**, *73*, 143–157. [CrossRef]
21. Li, D.; Zeng, D.; Yin, X.; Gao, D. Phase diagrams and thermochemical modeling of salt lake brine systems. III. Li_2SO_4 + H_2O, Na_2SO_4 + H_2O, K_2SO_4 + H_2O, $MgSO_4$ + H_2O and $CaSO_4$ + H_2O systems. *Calphad* **2018**, *60*, 163–176. [CrossRef]
22. Li, D.; Gao, D.; Dong, Y.; Li, W. Modeling of phase relations and thermodynamics in the $Mg(OH)_2$ + $MgSO_4$ + H_2O system with implications on magnesium hydroxide sulfate cement. *Calphad* **2019**, *67*, 101675. [CrossRef]